ACS Catalysis

Research Article

pubs.acs.org/acscatalysis

Reaction-driven Ion Exchange of Copper into Zeolite SSZ-13

A. K. S. Clemens,*[,†] A. Shishkin,[‡] P.-A. Carlsson,[‡] M. Skoglundh,[‡] F. J. Martínez-Casado,[§] Z. Matěj,[§] O. Balmes,[§] and H. Härelind*[,‡]

[†]Department of Applied Physics, Chalmers University of Technology, 412 96, Göteborg, Sweden

[‡]Department of Chemistry and Chemical Engineering, Competence Centre for Catalysis, Chalmers University of Technology, 412 96, Göteborg, Sweden

[§]MAX IV Laboratory, Lund University, 223 63 Lund, Sweden

Supporting Information

ABSTRACT: We have used several techniques to characterize Cu-SSZ-13 before and after exposure to reaction conditions relevant for NO reduction by NH_3−SCR to address the increase in NH_3−SCR activity observed as a function of time on stream. Specifically, we focus on characterizing copper species in samples prepared with solid state ion exchange (SSIE) having varying Cu loadings from 0.7 to 5.2 wt %. X-ray diffraction shows that CuO species that likely remain from the SSIE synthesis on the outside of the zeolite crystallites are significantly reduced by exposure to reaction conditions. High-resolution X-ray diffraction (HR-XRD) further reveals a corresponding increase of Cu_2O species. X-ray photoelectron, Auger electron, and ultraviolet−visible spectroscopy show an increase in both Cu(II) and Cu(I) species inside the zeolite pores, with a preserved long-range order of the zeolite structure as revealed by HR-XRD.

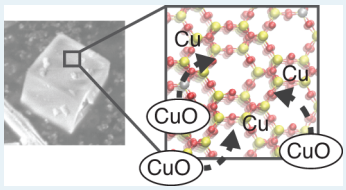

KEYWORDS: *NH_3−SCR, Cu-SSZ-13, diesel exhaust aftertreatment, solid-state ion-exchange, NO_x reduction*

1. INTRODUCTION

Zeolites are porous crystalline aluminosilicates with particular structural and chemical properties. They can be utilized for separation processes as molecular sieves,[1−3] for water softening applications in detergents,[4] and as catalysts for numerous chemical reactions.[2,5−8] One example of the latter is the selective catalytic reduction of nitrogen oxides (NO_x) with ammonia (NH_3−SCR) under oxygen excess conditions. This important technique is used to abate emissions of NO_x from both stationary and mobile sources.[9,10] Particularly promising are metal loaded small-pore zeolites with chabazite (CHA) structure, such as copper exchanged SSZ-13, which show high activity and selectivity toward N_2 formation in a broad temperature interval while exhibiting high hydrothermal stability during NH_3−SCR.[9,10]

Two common preparation methods of Cu-SSZ-13 are a one-pot synthesis using organo-copper complexes[11−13] and an aqueous ion-exchange (AIE) route following the synthesis of Na-SSZ-13.[14−21] For the AIE, the zeolite is suspended in an aqueous solution of a copper salt at specified conditions. The active catalytic species formed during AIE have been identified as isolated Cu^{2+} ions by the use of a multitude of techniques including X-ray diffraction (XRD),[14,22] neutron scattering,[16] temperature-programmed reduction (TPR),[23] and a number of spectroscopic methods such as UV−vis spectroscopy,[15,21] X-ray absorption spectroscopy (XAS),[16,24−27] electron spin resonance (EPR),[19,27] and infrared (IR) spectroscopy.[28] Although AIE is widely used, some drawbacks of this method can be identified. The procedure can be time-consuming and tedious because it involves washing and filtering steps that result in potentially harmful copper-containing waste solutions. In addition, the metal loading of the zeolite is often difficult to predict, and sometimes multiple exchange steps have to be performed in order to obtain the desired ion-exchange level. To circumvent some of the mentioned disadvantages of the AIE method, we employ here a solid-state ion-exchange (SSIE) procedure to introduce the active copper species into the zeolite. The SSIE method relies on heating a physical mixture of the zeolite and a copper salt to temperatures near 800 °C. Thereby copper ions migrate into the zeolite without the need of a solvent as a third component.[29] Another advantage of the SSIE route is that it is less time-consuming than the AIE. Further, it can allow the insertion of ions that in solution only exist as bulky aqueous complexes, which is of particular importance for ion exchange of small-pore zeolites. Recently, Wang et al.[30] reported on SSIE to prepare Cu-SSZ-13 and Shwan et al. investigated the effect of ammonia during low-temperature SSIE using copper oxide and zeolites of different framework structures.[31] Based on observations by scanning transmission electron microscopy (STEM) and XRD, the authors of the latter report concluded that the mobility of copper increases in the presence of ammonia during the SSIE.

In the present work, Cu-SSZ-13 ion-exchanged using SSIE is characterized to deepen the understanding of the nature of the different Cu species introduced into the zeolite pores and of how these species influence the NH_3−SCR activity. A series of Cu-SSZ-13 samples with varying Cu loadings is prepared by SSIE using copper acetate as a precursor. The nature of the

Received: June 9, 2015
Revised: August 28, 2015
Published: September 8, 2015

DOI: 10.1021/acscatal.5b01200
ACS Catal. 2015, 5, 6209−6218

present Cu species is investigated both before and after evaluation of the NH_3−SCR activity of the catalysts by X-ray fluorescence spectroscopy (XRF), XRD, scanning electron microscopy (SEM), UV−vis spectroscopy, X-ray photoelectron spectroscopy (XPS), as well as temperature-programmed desorption (TPD) of NH_3 and NO.

2. EXPERIMENTAL METHODS

2.1. Solid-State Ion-Exchange. H-SSZ-13 was synthesized following the procedures reported elsewhere,[14,18] resulting in a material with a Si/Al ratio of 13 as determined by X-ray fluorescence spectroscopy (see details below). For the SSIE, H-SSZ-13 was thoroughly physically mixed with copper(II)acetate monohydrate (CuAc, Merck) using a mortar. The CuAc content was varied from 2 to 15 wt % to result in the different Cu loadings specified in Table 1. To obtain Cu-SSZ-13, the mixed solids were transferred into an oven and first calcined in the air at 120 °C for 4 h followed by calcination at 600 °C for 5 h before the temperature was increased to 800 °C, at which the samples were kept for 12 h. The temperature increase between the steps was set to 2 °C min^{-1}.

Table 1. Overview over the Analysed Series of H-SSZ-13 and Five Cu-SSZ-13 Samples with Different Cu Loadings Prepared by SSIE

no	sample	wt % Cu	% IE
1	H-SSZ-13	0	0
2	Cu-SSZ-13	0.7	15
3	Cu-SSZ-13	2.0	50
4	Cu-SSZ-13	2.7	70
5	Cu-SSZ-13	3.7	100
6	Cu-SSZ-13	5.2	140

2.2. Catalytic Activity Measurements. The activity of the samples for the so-called *standard* NH_3−SCR reaction, *i.e.*, $4NH_3 + 4NO \rightarrow 4N_2 + 6H_2O$,[10] was measured in a continuous gas flow reactor system that has been previously described in detail in ref 18. Before the activity measurements, the powder samples were pressed to tablets and subsequently crushed and sieved to obtain a particle size between 630 μm and 1.0 mm. In each experiment, 50 mg of catalyst was used. The steady-state activity was investigated at temperatures between 150 and 500 °C using a gas mixture containing 400 ppm of NO, 400 ppm of NH_3, 8% O_2, and 5% H_2O in Ar. The total flow was kept constant at 300 mL min^{-1} resulting in a space velocity (GHSV) of 205 000 h^{-1}. The outlet gas composition was continuously analyzed using FTIR spectroscopy with an MKS 2030 FTIR spectrometer.

2.3. Catalyst Characterization. The elemental bulk composition of the samples was accessed by XRF using a PANalytical PW2424 instrument and the software UniQuant 5.0. The crystal structure of the samples was determined by XRD both in a Siemens D5000 diffractometer using Ni-filtered Cu Kα radiation (λ = 1.54187) and at the I711 beamline of Max II (MAX IV Laboratory, Lund, Sweden) giving high-resolution X-ray diffractograms. For the beamline experiments, samples were measured in transmission mode in 0.3 mm spinning capillaries using a Newport diffractometer equipped with a Pilatus 100 K area detector mounted 765 mm from the sample. The detector was scanned continuously, from 0 to 120° in approximately 6−10 min, recording 62.5 images/° (step size 0.016°) for each measurement. The true 2-Theta position of each pixel was recalculated, yielding an average number of 100 000 pixels contributing to each 2-Theta value. Integration, applying no corrections for the tilt of the detector, provided fwhm values of 0.03−0.08° from 0 to 120°. The Rietveld refinement was performed with the *FullProf*[32,33] program, using the model of the Cu-SSZ-13 by Fickel et al.[14] The unit cell of chabazite is hexagonal (space group $R\bar{3}m$). In all the cases, disordered water molecules were modeled in the pores of the structure of the chabazite with low occupancies (~0.25 in total). The main crystallographic data and experimental parameters of the measurements are given in Table S1. The morphology of the zeolite crystallites was examined using a LEO Ultra 55 SEM applying an acceleration voltage of 20 kV and a working distance of 10 mm. The chemical state of the Cu species in the zeolite samples was determined by X-ray photoelectron spectroscopy. The XPS measurements were obtained with a PerkinElmer PHI 5000C ESCA system using either monochromatic Al Kα or Mg Kα radiation. The powder samples were placed on a double-side adhesive carbon tape. Correction for charging was performed by shifting the binding energies (BE) using the C 1s peak at 287 eV as an internal reference that originates from the tape surface consisting of polycarbonates.[34,35] The presence of carbonyl and carboxyl groups in the carbon tape, fixating the sample, results in a shift of the C 1s peak to higher binding energies compared to the binding energy of 284.6 eV of carbon in graphitic materials. The X-ray photoelectron signal is presented as a function of the binding energy and normalized to the intensity of the Cu $2p_{3/2}$ peak at 933.2−933.6 eV to show the relative differences in peak height. The Auger signal is presented as a function of the kinetic energy (KE) and normalized to the intensity at 925 eV. The nature of the different Cu species was also examined by UV−vis spectroscopy using a Varian Cary 5000 instrument equipped with an integrating sphere detector (Internal DRA 2500).

Temperature-programmed desorption experiments with NO and NH_3 were performed after exposing the samples to the NH_3−SCR reaction gas mixture. NO-TPD was performed in a microcalorimeter (Setaram Sensys DSC) connected to a gas mixing system with Bronkhorst LOW-ΔP-FLOW mass flow controllers and a Hiden HPR-20 mass spectrometer for detection of the desorbing species. The powder sample (20 mg) was placed on a sintered quartz bed inside a quartz tube, and the total flow through the sample was set to 20 mL min^{-1}. The sample was first exposed to 500 ppm of NO at 150 °C for 4 h, and then the system was flushed with Ar for another 2 h. Finally, the temperature was linearly increased to 500 °C with a heating rate of 10 °C min^{-1}. NH_3-TPD was performed both in the microcalorimeter as well as in the flow reactor system described in the previous section. For measurements in the microcalorimeter, the sample was exposed to 500 ppm of NH_3 at 150 °C for 3.2 h. The NH_3-TPD was then performed in an analogous manner to the NO-TPD. To facilitate the deconvolution of the TPD spectra, in an additional experiment, the sample temperature was kept constant at 170 or 230 °C for 5 h after the NH_3 adsorption and a flushing step with Ar. Then, TPD spectra were recorded during a temperature increase to 500 °C with a heating rate of 10 °C min^{-1}. For measurements in the gas flow reactor, the same sample amounts and total flow as for the activity measurements were used. After exposure to 500 ppm of NH_3 at 150 °C for 4 h, the system was flushed with Ar for 45 min. The desorbing species during the subsequent temperature increase to 550 °C applying a heating rate of 10 °C

DOI: 10.1021/acscatal.5b01200
ACS Catal. 2015, 5, 6209−6218

min^{-1} were monitored by FTIR spectroscopy with an MKS 2030 FTIR spectrometer. In case of FTIR detection, the peak temperature was shifted by 25 °C to higher temperatures to adjust for a delay in detection caused by the setup of the FTIR instrument that consists of a 200 mL gas cell as opposed to the instant MS detection.

3. RESULTS AND DISCUSSION

In order to understand the nature of the different Cu sites, a series of Cu-SSZ-13 samples with different Cu loadings was prepared by SSIE and characterized both before and after measuring the NH_3−SCR activity. Before presenting and discussing the activity and characterization results in detail, we comment on the degree of Cu ion-exchange. With the assumption that all Cu ions are exchanged into the zeolite during the ion-exchange process, the theoretical ion-exchange level (IE) can be calculated by

$$\mathrm{IE} = \frac{2[\mathrm{Cu}]}{[\mathrm{Al}]}\% \quad (1)$$

where [Cu] and [Al] are the molar fractions of copper and aluminum, respectively. An ion-exchange level of 100% thus means that all theoretically available sites for Cu^{2+} are occupied, and levels above 100% refer to an overexchanged zeolite with external copper species present (outside the zeolite crystallites). This definition is commonly used for aqueous ion-exchanged samples where the inserted species has been uniquely identified as Cu^{2+} ions while external Cu species are usually not present at IE < 100%. In our case, we can observe varying amounts of external CuO, and hence the ion-exchange level can only be seen as the theoretically achievable maximum degree of ion exchange at a certain Cu content. This definition of the IE also implies that the total number of available Al is important. Hence, the lower the Si/Al ratio, the higher the Al content in the zeolite and the higher the number of Cu sites that are theoretically available in the zeolite. The loadings and IE of the investigated Cu-SSZ-13 samples are summarized in Table 1.

In Figure 1, the NO_x and NH_3 conversions during NH_3−SCR with the prepared H-SSZ-13 and Cu-SSZ-13 samples (0.7−5.2 wt % Cu) are shown. NO_x conversions as high as 94% could be obtained, which is comparable to previously reported conversions over both aqueous and solid-state ion-exchanged Cu-SSZ-13 catalysts.[17,30] In contrast to the findings for aqueous ion-exchanged Cu-SSZ-13 by Kwak et al., the NO_x and NH_3 conversions in the present study are observed to increase with increasing Cu loading without saturation. For the samples with Cu loadings higher than 2.7 wt %, a decrease in NO_x conversion is observed at temperatures above 300 °C, while the NH_3 conversion continues to increase. This has also been observed previously[23] and is likely due to direct oxidation of ammonia by oxygen, which is the major side reaction of NH_3−SCR favored at higher temperatures and by the presence of CuO. In Figure 2, the NO_x and NH_3 conversions of solid-state

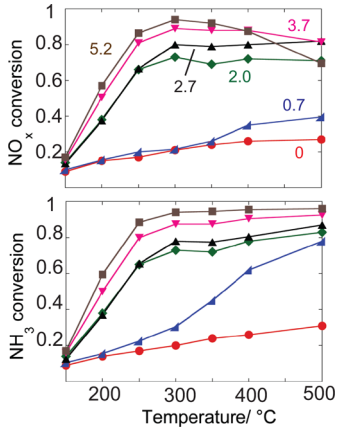

Figure 1. Catalytic activity for NH_3−SCR of H-SSZ-13 (0) and solid-state ion-exchanged Cu-SSZ-13 with Cu loadings between 0.7 and 5.2 wt %.

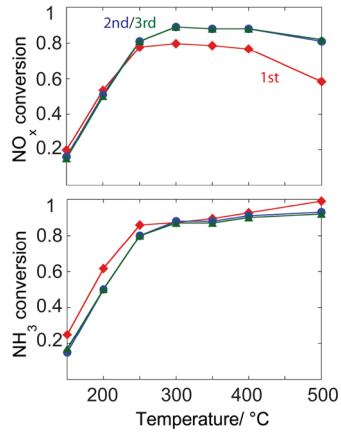

Figure 2. Catalytic activity for NH_3−SCR of solid-state ion-exchanged Cu-SSZ-13 containing 3.7 wt % Cu in the first, second, and third consequent experiments.

ion-exchanged Cu-SSZ-13 with 3.7 wt % Cu during NH_3−SCR in the first, second, and third subsequent experiment are shown. After the first catalytic experiment, the NO_x conversion is observed to increase by 9 and 22 percentage points at 300 and 500 °C, respectively. The NH_3 conversion, on the other hand, is between 2 and 12 percentage points lower in the second and third experiments, at each temperature. The same trend is also observed for the other samples (not shown). In order to understand the cause for this change in NH_3−SCR activity, the samples were characterized both before and after the first catalytic experiments.

The high-resolution XRD measurements (see Figure 3, Figure 4, and Table 2) confirm that the chabazite crystal structure of the zeolite[14] is maintained after the SSIE, which involves calcination at 800 °C for 12 h. A slight expansion of the unit cell of 0.4−0.5% is observed for the structures of the Cu-SSZ-13 samples compared to H-SSZ-13 likely due to insertion of Cu into the zeolite cages during the SSIE. The occupancy of Cu in the structure of the SSZ-13 samples is found to be small (0.03 in the sample with 2.0 wt % Cu and 0.02 in the sample with 5.2 wt % Cu). All Cu-SSZ-13 samples show an excess of CuO crystallites that are not incorporated in the zeolite crystallites. The amounts of CuO can be quantified to 1.9 and 5.4 wt % in the samples with 2.0 wt % Cu and 5.2 wt % Cu, respectively, before exposing them to NH_3−SCR reaction conditions. After the catalytic experiment, additionally, small amounts of Cu_2O (0.5−0.6 wt %) are clearly observed. The XRD reflexes of CuO are found to be significantly reduced by 10−60% depending on the Cu content, as shown in Figure 5. This suggests an insertion of the CuO present after the SSIE into the zeolite pores during the NH_3−SCR reaction. Shwan et al. have also observed this effect, and by a systematic testing of the reaction conditions during the SSIE, the authors propose

DOI: 10.1021/acscatal.5b01200
ACS Catal. 2015, 5, 6209−6218

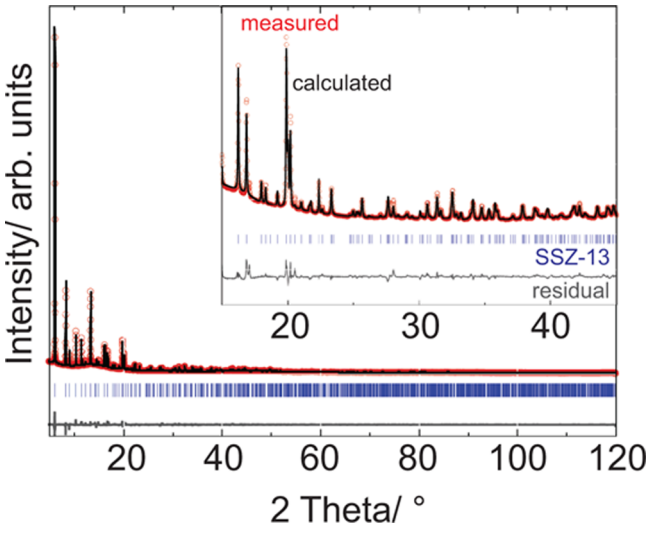

Figure 3. High-resolution XRD patterns of H-SSZ-13 used for the SSIE. The open red symbols show the measured values, the black line represents the calculated fit from the Rietveld refinement, and the gray line shows the difference between the measured and the calculated patterns. The position of the Bragg reflexes of SSZ-13 are marked with blue markers.

that ammonia transports Cu ions present outside the crystallites into the zeolite pores by forming a mobile linear diamine–Cu(I) complex.[31] Because of the oxidation state of this Cu complex, they suggest an increased presence of Cu(I) species in the solid-state ion-exchanged samples in contrast to aqueous ion-exchanged samples. We propose that the formation of the Cu(I)-complex also leads to the observed formation of Cu_2O species outside the zeolite crystallites.

The presence of external CuO species can also have an effect on the observed trend of continuosly increasing activity with increasing Cu content in the NH_3–SCR experiment (Figure 1). Whereas for aqueous ion-exchanged samples, the maximum loading of active Cu species can already be reached at an IE level of 40%,[23] we observe the highest activities for samples at IE levels between 100 and 140%. This suggests a lower insertion of active Cu(II) species for the same Cu content compared to samples prepared by AIE. It is worth noting that the SSZ-13 sample used for the AIE in the study by Kwak et al. exhibits a lower Si/Al ratio of 6 than the material used for SSIE (Si/Al = 13) in the present work. For the same IE, the total number of Cu species is thus higher in the samples prepared by AIE than in those prepared by SSIE. Nevertheless, even by taking into account the different Si/Al ratios, the observed difference between the aqueous- and solid-state ion exchanged samples in the increase of NO_x reduction activity relative to the increase of Cu content is significant.

A representative SEM image of the Cu-SSZ-13 sample containing 5.2 wt % Cu prepared by SSIE is shown in Figure 6. The observed cubic structures exhibit a morphology and crystallite size typical for SSZ-13.[14] The presence of external CuO, as indicated by the XRD measurements, could not be observed with certainty.

The elemental composition of the samples was determined by both XRF and XPS, and the results are presented in Table 3. When measured by XPS, surprisingly, the composition is observed to change slightly between before and after the NH_3–SCR reaction. However, one has to bear in mind that the XPS measurements are influenced both by the limited penetration depth of a few nanometres from the surface as well as by the dependence on the distribution of the species. This becomes especially apparent when no Cu could be detected by XPS for a

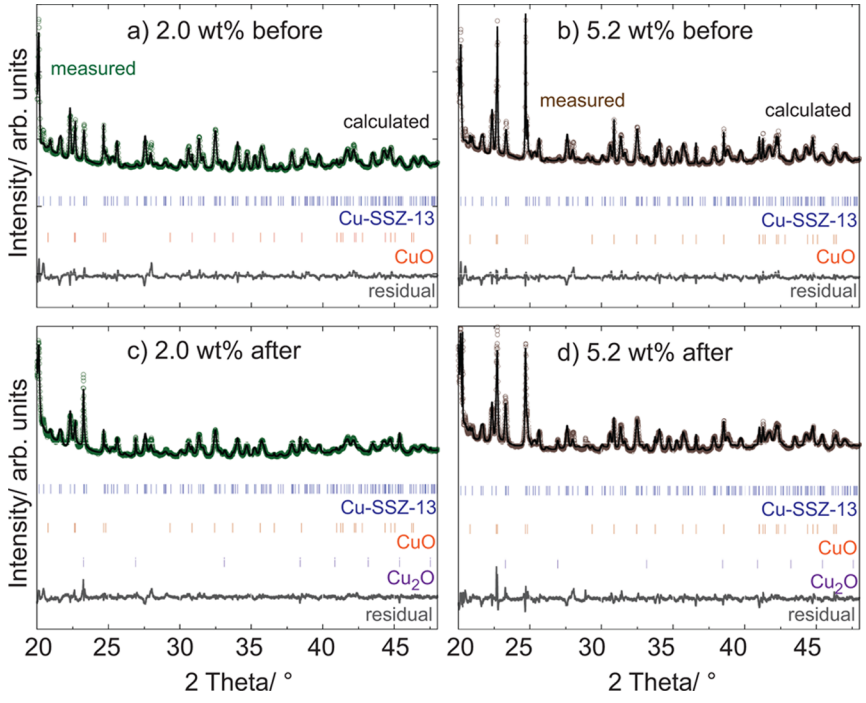

Figure 4. HR-XRD patterns of the Cu-SSZ-13 samples with Cu loadings of 2.0 (a, c) and 5.2 wt % (b, d) before (a, b) and after (c, d) the NH_3–SCR activity experiments. The open symbols show the measured values. The black lines represent the calculated fits from the Rietveld refinement, and the gray lines show the difference between the measured and the calculated patterns. The positions of the Bragg reflexes of Cu-SSZ-13, CuO, and Cu_2O are marked with blue, orange, and violet markers, respectively.

DOI: 10.1021/acscatal.5b01200
ACS Catal. 2015, 5, 6209–6218

Table 2. Crystallographic Data for the Samples Studied by High-Resolution XRD

samples		composition			a (Å)	c (Å)	volume (Å^3)
H-SSZ-13		SSZ-13			13.56068(17)	14.7539(3)	2349.64(6)
		Cu-SSZ-13:	CuO:	Cu_2O:			
Cu-SSZ-13	2.0 wt % Cu before	98.1%	1.9%		13.5841(3)	14.7802(5)	2361.97(11)
Cu-SSZ-13	2.0 wt % Cu after	98.2%	1.2%	0.6%	13.5795(3)	14.7807(5)	2360.42(11)
Cu-SSZ-13	5.2 wt % Cu before	94.6%	5.4%		13.5784(2)	14.7696(4)	2358.29(9)
Cu-SSZ-13	5.2 wt % Cu after	94.2%	5.3%	0.5%	13.5803(2)	14.7726(4)	2359.44(9)

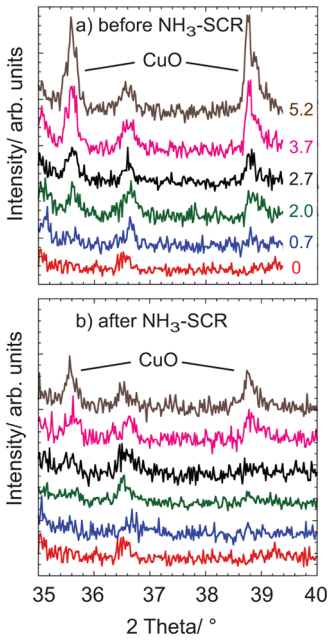

Figure 5. XRD patterns of H-SSZ-13 (0) and the Cu-SSZ-13 samples with Cu loadings between 0.7 and 5.2 wt % showing the peaks corresponding to CuO before (a) and after (b) the NH_3−SCR activity experiment.

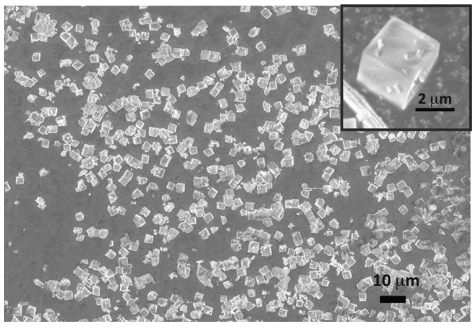

Figure 6. Representative SEM image of the solid-state ion-exchanged Cu-SSZ-13 sample containing 5.2 wt % Cu.

Table 3. Elemental Composition of the Cu-SSZ-13 Sample Containing 2.7 wt % Cu As Measured by XPS and XRF

	elemental composition (mol %)		
element	XPS before	XPS after NH_3−SCR	XRF
O	67.4	68.5	66.9
Si	27.7	27.2	30.9
Al	4.4	3.7	2.3
Cu	0.5	0.7	0.8
Cu/Si	0.018	0.026	0.026

H-SSZ-13/CuO physical mixture with the same Cu content as the Cu-SSZ-13 sample. This physical mixture was prepared by applying the same temperature treatment to both H-SSZ-13 and CuAc prior to mixing. In the physical mixture, the Cu is mainly present as external CuO species (as indicated by XRD measurements) that are not very well distributed throughout the sample. Therefore, the Cu content measured by XPS can become an indicator to which extent Cu is inserted into the zeolite when comparing the results to the XRF measurements that probe the bulk composition of the samples. When measured after the activity experiment, both XRF and XPS give the same Cu/Si ratio of the sample. This finding suggests that the clustered CuO species decrease after exposing the sample to NH_3−SCR conditions and that isolated Cu species detectable by XPS are inserted into the zeolite pores.

By XPS, the oxidation state of Cu in the zeolite samples was also characterized. In Figure 7, the Cu 2p XPS peak (left) and

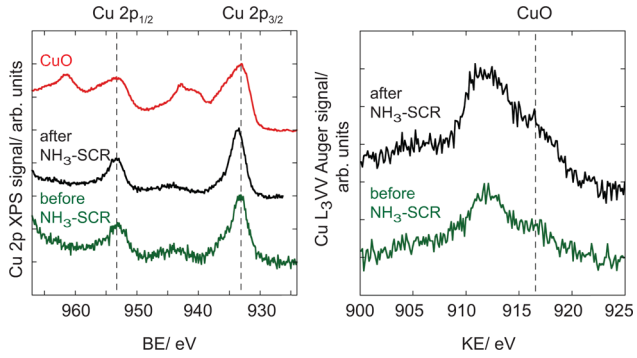

Figure 7. Left: XPS spectra of the Cu 2p core level for CuO and Cu-SSZ-13 loaded with 2.7 wt % Cu before and after the NH_3−SCR reaction. The positions of the Cu $2p_{3/2}$ and Cu $2p_{1/2}$ signals as measured for CuO are marked with dashed lines. Right: Cu L_3VV Auger signal for the Cu-SSZ-13 sample loaded with 2.7 wt % Cu before and after the NH_3−SCR reaction. The position of the highest intensity peak as measured for CuO is marked with the dashed line.

the X-ray induced Auger signal (right) of Cu $L_3M_{45}M_{45}$ (L_3VV) are shown for the Cu-SSZ-13 sample with 2.7 wt % Cu before and after the NH_3−SCR experiment, as well as for CuO. As mentioned before, for the physical mixture of CuO and H-SSZ-13, the XPS signal intensities for Cu are too low to be able to compare. In Table 4, the binding energies of Cu $2p_{3/2}$ and the kinetic energies of the highest intensity peak of the Cu L_3VV signal as well as the alpha parameter (α) are presented for the measured samples as well as for reference compounds reported in the literature. The alpha parameter is defined as follows:

$$\alpha = \mathrm{BE}(\mathrm{Cu2p_{3/2}}) + \mathrm{KE}(\mathrm{CuL_3VV}) \quad (2)$$

The Cu $2p_{3/2}$ energies for CuO and Cu-SSZ-13 before the NH_3−SCR experiments are observed to be identical, whereas a slight shift of 0.4 eV to higher BE could be determined for Cu-

DOI: 10.1021/acscatal.5b01200
ACS Catal. 2015, 5, 6209−6218

Table 4. Binding Energies (BE) of the Cu $2p_{3/2}$ XPS Signal, Kinetic Energies (KE) of the Cu L_3VV Auger Line, and the α Parameter for Samples of Cu-SSZ-13 Loaded with 2.7 wt % Cu Measured before and after the NH_3−SCR Reaction and for CuO, As Well As Literature Values for CuO, Cu_2O, and Cu Metal

		BE Cu $2p_{3/2}$ /eV	KE Cu L_3VV/ eV	α
measured	before NH_3−SCR	933.2	911.8	1845.0
	after NH_3−SCR	933.6	911.6	1845.2
	CuO	933.2	916.5	1849.7
literature	CuO[55]	933.8	917.9	1851.7
	Cu_2O[56]	932.4	916.8	1849.4
	Cu[57]	932.7	918.7	1851.3

SSZ-13 after the NH_3−SCR experiment. It has been stated previously[36] that the Cu $2p_{3/2}$ binding energies of Cu ions in the zeolite pores often are higher than for the corresponding oxides. Hence, the higher BE for Cu-SSZ-13 after the NH_3−SCR experiment is yet another indication of enhanced insertion of Cu into the zeolite pores after the reaction. Apart from the $2p_{3/2}$ and $2p_{1/2}$ peaks, Cu(II) species give rise to so-called shakeup lines at around 942 and 962 eV. The intensities of the shakeup lines for the ion-exchanged zeolites were found to decrease compared to CuO, which is significant for a loss of Cu(II) in octahedral coordination.[37] This can either indicate an increase of Cu(I) or Cu(0) species relative to Cu(II) or it can be caused by dehydration of the zeolite in the ultrahigh vacuum needed for the photoelectron spectroscopy measurements, which results in a tetrahedral coordination of Cu(II). Control experiments with short irradiation times of a few minutes show the same result ensuring that the intensity decrease of the shakeup lines is not caused by reduction of the Cu(II) species through the irradiation by X-rays.[37]

Additionally, the Cu L_3VV Auger line can be used as a probe for the oxidation state of Cu. For the Cu-SSZ-13 samples, a significant shift of more than 5 eV to lower KE is observed as compared to CuO. The values for CuO, Cu_2O, and Cu that are reported in the literature (shown in Table 4) are in the same range as the one measured for CuO. Because the Cu $2p_{3/2}$ binding energy also varies with the oxidation state, a comparison of the Auger parameter α can help in distinguishing the oxidation states. However, here α is 4−6 eV lower than for the Cu references due to the significant shift of the Cu L_3VV KE. One possible reason for the shift of the Auger line is the different polarizibility of the Cu−O−Si bond present in a Cu ion-exchanged zeolite compared to the Cu−O−Cu bonds found in CuO. A similar shift has also been observed by Liese et al. for Cu-ZSM-5 who used the magnitude of this shift as a measure for the incorporation of Cu into the zeolite pores.[38] The KE of the line is very similar for both Cu-SSZ-13 before and after the NH_3−SCR experiment, but the shoulder at 916.5 eV that is observed for both samples at the maximum of the highest intensity peak of CuO is found to be higher for the fresh sample. This is indicative of a higher CuO amount in the sample before the NH_3−SCR reaction. Furthermore, the Auger peak for the sample after the activity experiment is broader and suggests a contribution of two different species. A possible explanation is the presence of both Cu^+ and Cu^{2+} ions in the zeolite after the NH_3−SCR experiment as the KE of Cu(I) and Cu(II) species are only separated by around 1 eV (see Table 4).

UV−vis spectroscopy probes the electronic transitions of the Cu ion-exchanged zeolite and can thereby be helpful to distinguish the different Cu species present in the samples. The obtained UV−vis spectra are presented in Figure 8a for Cu-SSZ-13 with 2.7 wt % Cu as a physical mixture, before, as well as after, the NH_3−SCR experiment and compared with the spectra of pure CuO. The spectra for Cu-SSZ-13 with Cu loadings between 0.7 and 5.2 wt % are shown in Figure 8b before and in Figure 8c after the activity experiment. For all spectra except for CuO, the absorbance of H-SSZ-13 is subtracted in order to only show the contributions of the Cu species. CuO gives rise to a broad absorption across the entire UV and visible region of the spectrum that decreases at wavelengths higher than 800 nm. As expected, these characteristics are also represented with lower intensity in the spectrum of the physical H-SSZ-13/CuO mixture. In contrast, the spectra of Cu-SSZ-13 before and after the NH_3−SCR reaction are different and indicate a change from the pure CuO contribution both after the SSIE (before the NH_3−SCR experiment) and after the reaction. The absorption features of the Cu-SSZ-13 samples are broad but can be deconvoluted with six different peaks, see Figure 8d. An attempt was made to assign the different peaks to different Cu species and transitions assisted by assignments reported in the literature,[39−45] as shown in Table 5. It is important to note that such an assignment is difficult, due to the high number of transitions in Cu systems, as well as the broad and overlapping nature of the peaks. For aqueous ion-exchanged samples, absorbance peaks in two different wavelength ranges have been reported in the literature.[15,16,21] They correspond to peaks 1 and 2 as well as to peaks 5 and 6 in the present study and can be assigned to Cu(II) species. In contrast to the findings for aqueous ion-exchanged samples, we observe the two additional peaks 3 and 4, indicating the presence of additional Cu species in the solid-state ion exchanged Cu-SSZ-13, possibly Cu(I). The area of all peaks was observed to increase after using the samples for NH_3−SCR, with the exception of the sample with the lowest Cu concentration, indicating a chemical change of the system during the reaction.

NH_3-TPD experiments were performed with the aim to quantify both the remaining proton (H^+) as well as the active Cu sites in the samples after the activity experiment. The NH_3-TPD spectra for the H-SSZ-13 and Cu-SSZ-13 samples (0.7−5.2 wt %) are shown in Figure 9a. Multiple overlapping peaks were observed in the spectra that do not allow to draw conclusions about the amount of different sites without deconvolution. A contribution of three different peaks to the spectra seems probable for the Cu-SSZ-13 samples. In order to assist the peak deconvolution, additional TPD experiments starting at higher temperatures were performed. Due to practical reasons, the measurements were performed in a different system with MS detection. The resulting TPD spectra are presented in Figure 9b. The TPD profile labeled with 170 °C shows contributions of two peaks, denoted as B and C, and the TPD profile labeled with 230 °C only shows the contribution of peak C. Gaussian functions were fitted to the remaining peaks B and C as an approximation to the desorption peaks, which were then used to also fit peak A to the regular TPD profile (marked as 150 °C in Figure 9b). The obtained peak temperatures, peak areas, and peak widths were used to fit three peaks to the TPD spectrum of Cu-SSZ-13 with 2.7 wt % Cu obtained with FTIR detection, and an excellent fit to the experimental values could be obtained, see Figure 9c. This

DOI: 10.1021/acscatal.5b01200
ACS Catal. 2015, 5, 6209−6218

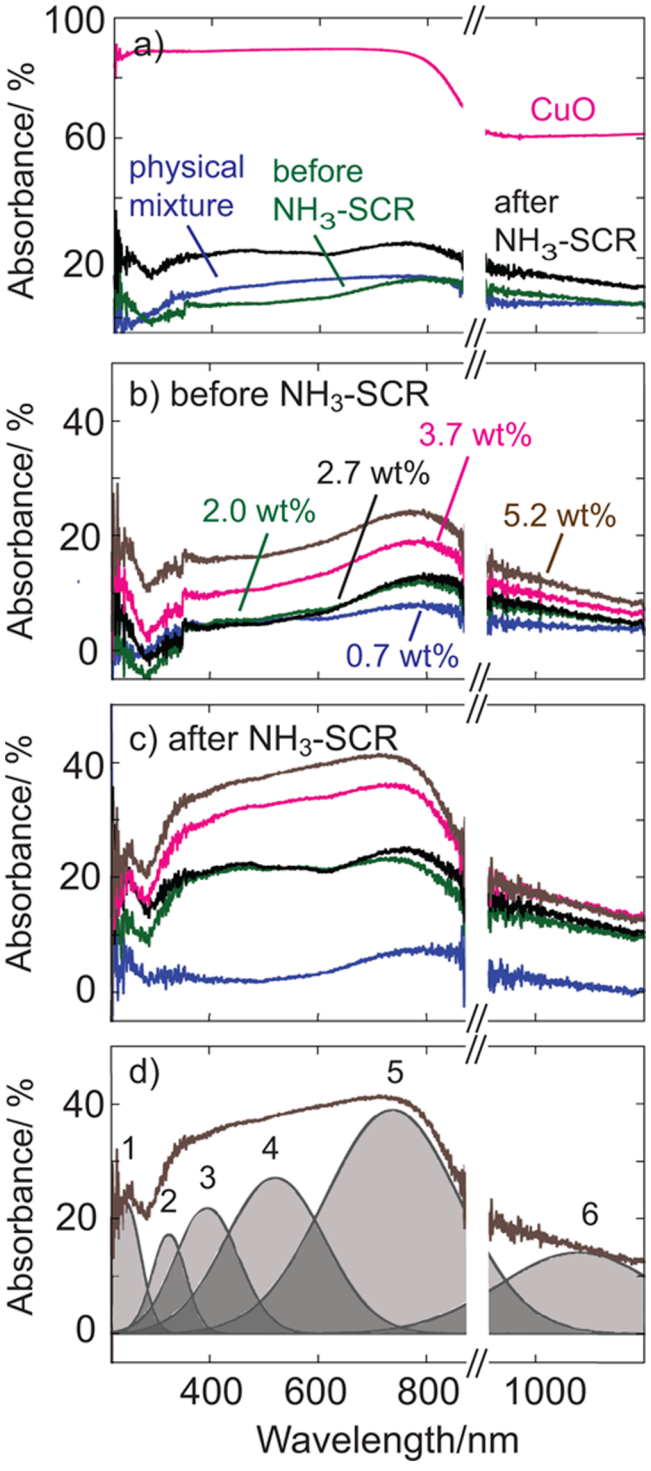

Figure 8. (a) UV−vis spectra for Cu-SSZ-13 loaded with 2.7 wt % Cu before and after the NH_3−SCR reaction, for the corresponding physical mixture of H-SSZ-13/CuO, and for CuO. For all spectra except CuO, the absorbance of H-SSZ-13 is subtracted showing only the contribution of the Cu species. (b,c) UV−vis spectra of Cu-SSZ-13 with Cu loadings between 0.7 and 5.2 wt % before and after the NH_3−SCR reaction. (d) Deconvolution of the spectra with six different peaks exemplarily shown for the Cu-SSZ-13 sample with 5.2 wt % after NH_3−SCR. Note that the noise in the spectra around 900 nm is due to a change of the detector grating.

deconvolution procedure results in excellent fits of the TPD spectra for all Cu-SSZ-13 samples shown in Figure 9. For the

Table 5. Possible Origin of the Deconvoluted Peaks of the UV−Vis Spectra Shown in ref 8

peak	wavelength/ nm	assignment
1	230−250	charge-transfer transition $O^{2-} \rightarrow Cu^{2+}$[39]
		$d^{10}-d^9s^1$ transition of Cu^+[39−41]
2	320−360	charge-transfer transition $O^{2-} \rightarrow Cu^{2+}$[41−44]
3	400−430	Cu^+ in 3d clusters in CuO[39]
		charge-transfer of O−Cu−O[40]
4	520−550	Cu^{2+} in $CuAl_2O_4$-like phase[40]
		plasmonic Cu_n nanoparticles[40]
5	730−790	d−d transition of Cu^{2+} in octahedral coordination[39,45]
6	1060−1100	d−d transition of Cu^{2+} in tetrahedral coordination[39]

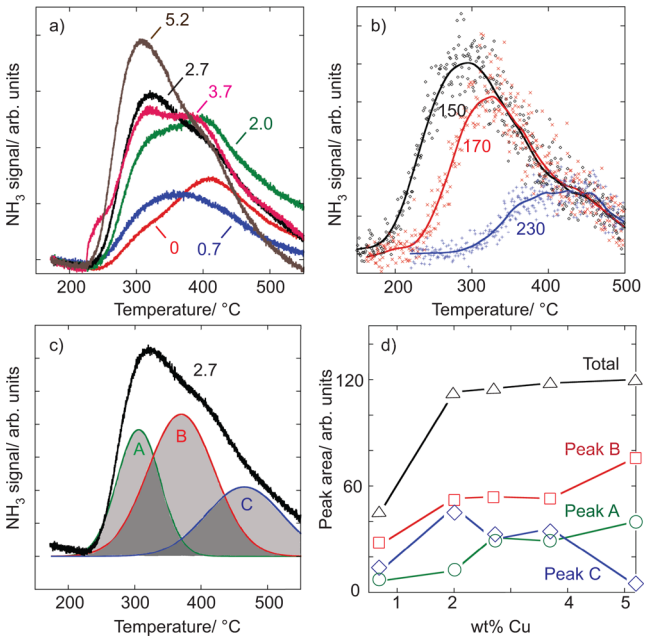

Figure 9. (a) NH_3-TPD spectra (FT-IR detection) after ammonia adsorption at 150 °C of H-SSZ-13 (0) and Cu-SSZ-13 with Cu loadings between 0.7−5.2 wt % after the NH_3 activity experiment. (b) NH_3-TPD spectrum (MS detection) of the Cu-SSZ-13 sample loaded with 2.7 wt % Cu recorded after NH_3 adsorption at 150 °C, as well as after adsorption and subsequent isothermal desorption of NH_3 at 170 and 230 °C. (c) Deconvoluted peaks A, B, and C for the NH_3-TPD spectra of Cu-SSZ-13 sample with 2.7 wt % Cu shown in a by using the relative peak temperatures and/or areas of the peaks in b. (d) Peak areas of the deconvoluted peaks A, B, and the C as well as the total peak area at all investigated Cu loadings.

H-SSZ-13 sample, however, no good fit could be obtained. This indicates that the peaks A−C are mainly associated with Cu sites and that other types of sites are present in the unexchanged zeolite. Generally, it is assumed that low-temperature Lewis acid sites (Cu^+, Cu^{2+}) are introduced in the zeolite at the expense of high-temperature Brønsted acid (H^+) sites.[30] However, the interpretation of the NH_3-TPD spectra seems more complex when considering the possible presence of Brønsted acid sites of different acidity, which depend on the location of the OH group within the zeolite.[46] Furthermore, Brønsted acid sites can become Lewis acid sites after adsorption of an additional NH_3 molecule in the form of $NH_3-H^+-NH_3$.[46] An additional complication comes through the porous nature of zeolites that makes diffusion and readsorption of NH_3 adsorbed to different sites likely.[47−49]

DOI: 10.1021/acscatal.5b01200
ACS Catal. 2015, 5, 6209−6218

Moreover, the location of the Cu sites could be modified in the course of a TPD experiment because it has been proposed that NH_3 can affect the mobility of Cu ions within the zeolite.[31] Despite all these complications regarding the analysis of the NH_3-TPD data, some general conclusions can be drawn by analyzing the peak areas of peaks A−C and the total peak area for all Cu concentrations, see Figure 9d. The total peak area is observed to increase with increasing Cu content because a Cu site can coordinate a higher number of NH_3 molecules compared to a proton site.[30] The largest increase was found between Cu loadings of 0.7 and 2 wt %, which suggests that the majority of binding sites for NH_3 are created at Cu loadings of around 2 wt %. This is in agreement with the considerable increase in NH_3−SCR activity for Cu loadings above 0.7 w%, cf. Figure 1, suggesting that the highest number of the most active Cu sites are obtained for copper loadings between 0.7 and 2 wt %. Peaks A and B both appear to increase with increasing Cu content, which likely is associated with two different Cu (Lewis acid) sites likely in contrast to the commonly assumed assignment of peak B to Brønsted acid sites.[30] Even if a contribution of H^+ sites to peak B is assumed, its maximum amount should be at the lowest Cu concentration and decrease with increasing Cu content. Consequently, even if the contributions of Brønsted acid sites could be subtracted from peak B, it is still found to increase with increasing Cu content. Also for Cu contents above the theoretical ion-exchange level of 100% (corresponding to the Cu concentration of 3.7 wt %, see Table 1), the number of Lewis acid sites (peak A and B) is still observed to increase. This indicates that not only Cu^{2+} but also Cu^+ species are exchanged into the zeolite, which increases the number of possible Cu sites. It also indicates the presence of CuO outside the zeolite pores, in line with the XRD measurements. Peak C is observed to first increase and then decrease with increasing Cu content. This can be indicative of a contribution of Brønsted acid sites to this peak. Another possibility is its relation to kinetic effects, such as diffusion limitations and readsorption issues introduced by the zeolite pore structure that can lead to an appearance of the peak at higher temperatures than expected based on the acid strength of the site. These effects make it difficult to assign peak C to a specific site within the zeolite.

The likely presence of Cu(I) species as observed by XPS, UV−vis spectroscopic, and NH_3-TPD measurements presents a further explanation to our observation that for reaching the same NH_3−SCR activity (cf. Figure 1) higher amounts of Cu have to be used in the SSIE compared to the AIE. This is because the AIE almost solely introduces the NH_3−SCR active species Cu(II), whereas by SSIE probably both Cu(II) and Cu(I) can be introduced in addition to the presence of external CuO species.

TPD measurements with NO represent a way to reveal the different Cu sites in the zeolite samples as NO binds exclusively to the metal sites in the zeolite. For all samples except H-SSZ-13 and Cu-SSZ-13 with 0.7 wt % Cu, desorption of NO, O_2, and N_2 could be detected during the TPD measurement. Desorption of NO_2 is found to be negligible for all samples, whereas NO desorbs in two distinct peaks at temperatures around 220 and 370 °C. Desorption of O_2 and N_2 is observed at the same temperature as for the second NO peak. The integrated peak areas and the molar ratio of NO to Cu derived from the NO-TPD experiments are shown in Table 6. The NO-TPD results are generally consistent with findings for other Cu zeolites published in the literature.[51−54] The first desorption peak at 220 °C is commonly assigned to desorption of NO from Cu(II) or Cu(I) sites inside the zeolites. The second desorption peak at 370 °C has been found to originate from desorption of NO from both isolated Cu(II) species and CuO aggregates where NO can be adsorbed in the form of nitrate (NO_3^-), nitrite (NO_2^-), or nitronium ion (NO_2^+) species.[52,53] Due to the decomposition of these complexes, desorption of O_2 (accompanied by N_2) is observed simultaneously with the NO desorption. In other studies, an additional NO peak was observed at a temperature of around 100 °C[51−54] that is lower than the adsorption temperature of NO used in the present study. The peak area of the first NO peak is found to decrease with a small exception for the samples between 2.7 and 3.7 wt % Cu. This likely means that this Cu binding site is less favorable than those corresponding to the second NO peak or the peak at 100 °C that could not be measured here. The second desorption peak of NO seems to generally increase with increasing Cu content, although the increase is not observed to be consistent with the increase in Cu. In contrast, this was the case for the O_2 desorption peak that was found to uniformly increase with increasing Cu content. This is consistent with the assignment to both internal Cu and external CuO sites that are more abundant for higher Cu contents. The total NO desorption is observed to increase for samples up to 3.7 wt % Cu and then to decrease for the 5.2 wt % Cu sample. Theoretically, an increase in adsorbed NO is expected with increasing Cu content. In our measurements, this does not seem to be the case, which becomes evident when taking the NO/Cu ratios into account.

Table 6. Peak Areas of the Desorbed Species from the Different Cu-SSZ-13 Samples during NO-TPD Measurements

Cu content wt %	NO peak 1×10^{-7} mol	NO peak 2×10^{-7} mol	NO total 10^{-7} mol	NO/Cu mol/mol	O_2 peak 10^{-10} mbar
0.7	–	–	–	0	–
2	7.7	3.2	11	0.17	1.7
2.7	6.0	2.3	8.3	0.10	4.3
3.7	6.3	10.1	16.4	0.14	7.4
5.2	3.7	7.8	11.5	0.07	7.6

By applying different characterization techniques, we could obtain information about the active sites in Cu-SSZ-13 prepared using solid-state ion exchange. Predominantly, Cu^{2+} species are observed, which is in line with the high NH_3−SCR activity besides the probable presence of Cu^+ species inside the zeolite. External CuO present after the SSIE is found to migrate into the zeolite pores during the NH_3−SCR reaction, increasing the activity for NO_x reduction. The procedure was found less time-consuming and more environmentally friendly compared to the commonly used approach of aqueous ion exchange. Based on these findings, we can suggest the SSIE as an alternative method to introduce Cu ions into a SSZ-13 pores. As an outlook for future studies, we see potential for further development of the SSIE preparation method for Cu-SSZ-13 by (i) enhancing the distribution of the Cu salt in the physical mixture with the zeolite by a more thoroughly physical mixing using, e.g., a vaporizable liquid during the grinding in a mortar, or a milling procedure, (ii) reducing the temperature of the SSIE as shown by Shwan et al.,[31] or (iii) investigating the influence of stream gases over the ion exchange reaction mixture, which has started to be investigated by Shwan et al.[31] It could be particularly interesting to extend the study to other

DOI: 10.1021/acscatal.5b01200
ACS Catal. 2015, 5, 6209−6218

gases and gas mixtures than those used in NH_3−SCR. We also see a potential in additional characterization studies in order to, for example, verify the presence of Cu^+ and to quantify the ratio between Cu^{2+} and Cu^+ species in the solid-state ion-exchanged materials.

4. CONCLUSIONS

In this study, the connection between the nature of the different Cu species introduced into the zeolite pores and the NH_3−SCR activity is investigated for solid-state ion-exchanged Cu-SSZ-13 with varying Cu content. High-resolution XRD shows a significant expansion of the SSZ-13 unit cell after the SSIE owing to copper insertion. By XRD, XPS, Auger electron, and UV−vis spectroscopy, as well as NH_3-TPD, it is found that fewer CuO species are present outside the zeolite crystallites after exposure to NH_3−SCR conditions, while we observe an increase of both Cu(II) and Cu(I) species inside the zeolite pores. These species likely originate from external CuO that is present after the SSIE. The high-resolution XRD measurements both confirm the existence of Cu_2O species and reveal that the increase in Cu(I) and Cu(II) species inside the zeolite pores occurs with preserved long-range order of the zeolite structure. We suggest that the observed improvement of the NH_3−SCR activity is owing to a reaction-driven insertion of Cu species into the zeolite pores.

■ ASSOCIATED CONTENT

Supporting Information

The Supporting Information is available free of charge on the ACS Publications website at DOI: 10.1021/acscatal.5b01200.

Complete spectra, experimental parameters, and main crystallographic data for the samples studied by HR-XRD (PDF)

■ AUTHOR INFORMATION

Corresponding Authors

*E-mail: anna.clemens@chalmers.se.
*E-mail: hanna.harelind@chalmers.se.

Notes

The authors declare no competing financial interest.

■ ACKNOWLEDGMENTS

Lars Ilver is acknowledged for his valuable advice during the XPS measurements. This work has been performed within the Competence Center for Catalysis which is funded by the Swedish Energy Agency, Chalmers University of Technology and the member companies: AB Volvo, ECAPS AB, Haldor Topsøe A/S, Scania CV AB, Volvo Car Corporation AB, and Wärtsilä Finland Oy. Financial support from Knut and Alice Walllenberg Foundation, Drn KAW 2005.0055, is acknowledged.

■ REFERENCES

(1) Sircar, S.; Myers, A. L. In *Handbook of Zeolite Science and Technology*; Auerbach, S. M., Carrado, K. A., Dutta, P. K., Eds.; Marcel Dekker Inc: New York, 2003; pp 1063−1104.
(2) Kulprathipanja, S.; James, R. B. In *Zeolites in Industrial Separation and Catalysis*; Kulprathipanja, S., Ed.; Wiley-VCH: New York, 2010; pp 173−202.
(3) De Baerdemaeker, T.; De Vos, D. *Nat. Chem.* **2013**, *5*, 89−90.
(4) Zatta, A.; Clerici, R.; Faccetti, E.; Mattioli, P.; Rabaioli, M. R.; Radici, P.; Aiello, R.; Crea, F. *Journadas del Comite Español de la Detergencia* **1997**, *27*, 71−82.
(5) Taylor, R. J.; Petty, R. H. *Appl. Catal., A* **1994**, *119*, 121−138.
(6) Miller, S.; Rosenbaum, J. *U.S. pat.* 2005, No. US6962651.
(7) Čejka, J., Corma, A., Zones, S., Eds. *Zeolites and Catalysis*; Wiley-VCH, 2010; Vol. 2; pp 547−861.
(8) Moliner, M.; Martínez, C.; Corma, A. *Angew. Chem., Int. Ed.* **2015**, *54*, 3560−3579.
(9) Beale, A. M.; Gao, F.; Lezcano-Gonzalez, I.; Peden, C. H. F.; Szanyi, J. *Chem. Soc. Rev.* **2015**, DOI: 10.1039/C5CS00108K. In press
(10) Gao, F.; Kwak, J. H.; Szanyi, J.; Peden, C. H. F. *Top. Catal.* **2013**, *56*, 1441−1459.
(11) Ren, L.; Zhu, L.; Yang, C.; Chen, Y.; Sun, Q.; Zhang, H.; Li, C.; Nawaz, F.; Meng, X.; Xiao, F.-S. *Chem. Commun.* **2011**, *47*, 9789−9791.
(12) Martínez-Franco, R.; Moliner, M.; Concepcion, P.; Thogersen, J. R.; Corma, A. *J. Catal.* **2014**, *314*, 73−82.
(13) Martínez-Franco, R.; Moliner, M.; Thogersen, J. R.; Corma, A. *ChemCatChem* **2013**, *5*, 3316−3323.
(14) Fickel, D. W.; Lobo, R. F. *J. Phys. Chem. C* **2010**, *114*, 1633−1640.
(15) Korhonen, S. T.; Fickel, D. W.; Lobo, R. F.; Weckhuysen, B. M.; Beale, A. M. *Chem. Commun.* **2011**, *47*, 800−802.
(16) Deka, U.; Juhin, A.; Eilertsen, E. A.; Emerich, H.; Green, M. A.; Korhonen, S. T.; Weckhuysen, B. M.; Beale, A. M. *J. Phys. Chem. C* **2012**, *116*, 4809−4818.
(17) Kwak, J. H.; Tran, D.; Szanyi, J.; Peden, C. H. F.; Lee, J. H. *Catal. Lett.* **2012**, *142*, 295−301.
(18) Shishkin, A.; Kannisto, H.; Carlsson, P.-A.; Härelind, H.; Skoglundh, M. *Catal. Sci. Technol.* **2014**, *4*, 3917−3926.
(19) Gao, F.; Walter, E. D.; Karp, E. M.; Luo, J.; Tonkyn, R. G.; Kwak, J. H.; Szanyi, J.; Peden, C. H. F. *J. Catal.* **2013**, *300*, 20−29.
(20) Zhu, H.; Kwak, J. H.; Peden, C. H. F.; Szanyi, J. *Catal. Today* **2013**, *205*, 16−23.
(21) Bates, S. A.; Verma, A. A.; Paolucci, C.; Parekh, A. A.; Anggara, T.; Yezerets, A.; Schneider, W. F.; Miller, J. T.; Delgass, W. N.; Ribeiro, F. H. *J. Catal.* **2014**, *312*, 87−97.
(22) Shin, N. R.; Kim, S. H.; Shin, H. S.; Jang, I. J.; Cho, S. J. *J. Nanosci. Nanotechnol.* **2013**, *13*, 4346−4349.
(23) Hun Kwak, J. H.; Zhu, H.; Lee, J. H.; Peden, C. H. F.; Szanyi, J. *Chem. Commun.* **2012**, *48*, 4758−4760.
(24) Kispersky, V. F.; Kropf, A. J.; Ribeiro, F. H.; Miller, J. T. *Phys. Chem. Chem. Phys.* **2012**, *14*, 2229−2238.
(25) McEwen, J.-S.; Anggara, T.; Schneider, W. F.; Kispersky, V. F.; Miller, J. T.; Delgass, W. N.; Ribeiro, F. H. *Catal. Today* **2012**, *184*, 129−144.
(26) Giordanino, F.; Borfecchia, E.; Lomachenko, K. A.; Lazzarini, A.; Agostini, G.; Gallo, E.; Soldatov, A. V.; Beato, P.; Bordiga, S.; Lamberti, C. *J. Phys. Chem. Lett.* **2014**, *5*, 1552−1559.
(27) Janssens, T. V. W.; Falsig, H.; Lundegaard, L. F.; Vennestrom, S. B.; Rasmussen, P. N. R.; Moses, P. G.; Giordanino, F.; Borfecchia, E.; Lomachenko, K. A.; Lamberti, C.; Bordigo, S.; Godiksen, A.; Mossin, S.; Beato, P. *ACS Catal.* **2015**, *5*, 2832−2845.
(28) Szanyi, J.; Kwak, J. H.; Zhu, H.; Peden, C. H. F. *Phys. Chem. Chem. Phys.* **2013**, *15*, 2368−2380.
(29) Karge, H. G.; Beyer, H. K. In *Post-Synthesis Modification I, Molecular Sieves*; Karge, H. G., Weitkamp, J., Eds.; Springer-Verlag: Berlin, 2002; Vol. 3; pp 47−201.
(30) Wang, D.; Gao, F.; Peden, C. H. F.; Li, J.; Kamasamudram, K.; Epling, W. S. *ChemCatChem* **2014**, *6*, 1579−1583.
(31) Shwan, S.; Skoglundh, M.; Lundegaard, L. F.; Tiruvalam, R. R.; Janssens, T. V. W.; Carlsson, A.; Vennestrom, P. N. R. *ACS Catal.* **2015**, *5*, 16−19.
(32) Rodríguez-Carvajal, J. *Phys. B (Amsterdam, Neth.)* **1993**, *192*, 55−69.
(33) Rodríguez-Carvajal, J. *Newsletter*; Commission on Powder Diffraction (IUCr): Chester, England, 2000; Vol. 26, pp 12−19.
(34) Barr, T. L.; Seal, S. *J. Vac. Sci. Technol., A* **1995**, *13*, 1239−1246.

DOI: 10.1021/acscatal.5b01200
ACS Catal. 2015, 5, 6209−6218

(35) Hyun, Y.; Kim, H.; Lee, C.-S. *Bull. Korean Chem. Soc.* **2012**, *33*, 3177−3183.
(36) Shpiro, E. S.; Grünert, W.; Joyner, R. W.; Baeva, G. N. *Catal. Lett.* **1994**, *24*, 159−169.
(37) Jirka, I.; Bosacek, V. *Zeolites* **1991**, *11*, 77−80.
(38) Liese, T.; Grünert, W. *J. Catal.* **1997**, *172*, 34−45.
(39) Praliaud, H.; Mikhailenko, S.; Chajar, Z.; Primet, M. *Appl. Catal., B* **1998**, *16*, 359−374.
(40) Pestryakov, A. N.; Petrnovskii, V. P.; Kryazhov, A.; Ozhereliev, O.; Pfänder, N.; Knop-Gericke, A. *Chem. Phys. Lett.* **2004**, *385*, 173−176.
(41) Nunes Amorim de Carvalho, M. C.; Barboza Passos, F.; Schmal, M. *Appl. Catal., A* **2000**, *193*, 265−276.
(42) Itho, Y.; Nishiyama, S.; Tsuruya, S.; Masai, M. *J. Phys. Chem.* **1994**, *98*, 960−967.
(43) Spoto, G.; Zecchina, A.; Bordiga, S.; Ricchiardi, G.; Martra, G. *Appl. Catal., B* **1994**, *3*, 151−172.
(44) Liang, C.; Li, X.; Qu, Z.; Tade, M.; Liu, S. *Appl. Surf. Sci.* **2012**, *258*, 3738−3743.
(45) Schoonheydt, R. A. *Catal. Rev.: Sci. Eng.* **1993**, *35*, 129−168.
(46) Valyon, J.; Onyestyak, G.; Rees, V. C. *J. Phys. Chem. B* **1998**, *102*, 8994−9001.
(47) Palermo, A.; Aldao, C. M. *Thermochim. Acta* **1998**, *319*, 177−184.
(48) Niwa, M.; Katada, N. *Catal. Surv. Jpn.* **1997**, *1*, 215−226.
(49) Forni, L.; Vatti, F. P.; Ortoleva, E. *Microporous Mater.* **1995**, *3*, 367−375.
(50) Komatsu, T.; Nunokawa, M.; Moon, I. S.; Takahara, T.; Namba, S.; Yashima, T. *J. Catal.* **1994**, *148*, 427−437.
(51) Zhang, W.-X.; Yahiro, H.; Mizuno, N.; Izumi, J.; Iwamoto, M. *Langmuir* **1993**, *9*, 2337−2343.
(52) Shimokawabe, M.; Hatakeyama, N.; Shimada, K.; Tadokoro, K.; Takezawa, N. *Appl. Catal., A* **1992**, *87*, 205−218.
(53) Torre-Abreu, C.; Ribeiro, M. F.; Henriques, C.; Delahay, G. *Appl. Catal., B* **1997**, *12*, 249−262.
(54) Tounsi, H.; Djemel, S.; Ghorbel, A.; Delahay, G. *J. Soc. Chim. Tunis.* **2007**, *9*, 85−96.
(55) Wagner, C. D.; Riggs, W. M.; Davis, L. E.; F, M. J.; Muilenberg, G. E. *Handbook of X-ray Photoelectron Spectroscopy*; Physical Electronics Division, Perkin Elmer Corporation: Eden Prairie, MN, 1992; Vol. *1*; pp 86−87.
(56) Tobin, J. P.; Hirschwald, W.; Cunningham, J. *Appl. Surf. Sci.* **1983**, *16*, 441−452.
(57) Anthony, M. T.; Seah, M. P. *Surf. Interface Anal.* **1984**, *6*, 95−106.

DOI: 10.1021/acscatal.5b01200
ACS Catal. 2015, 5, 6209−6218